Eur. Phys. J. D (2017) 71: 76
DOI: 10.1140/epjd/e2017-70732-7

THE EUROPEAN PHYSICAL JOURNAL D

Regular Article

Optical emission in the dissociation of ammonia by low energy He^+ ions

Ryszard Drozdowski, Slawomir Werbowy[a], Łukasz M. Sobolewski, and Andrzej Kowalski

Institute of Experimental Physics, Faculty of Mathematics, Physics, and Informatics, University of Gdansk, ul. Wita Stwosza 57, 80-308 Gdansk, Poland

Received 22 November 2016 / Received in final form 19 January 2017
Published online 28 March 2017

Abstract. Molecular bands associated with the ND(A-X), ND(c-a), ND^+(B-X), and ND^+(C-X) transitions, as well as atomic lines of Balmer series and several He and He^+ lines, were observed in the collisions of He^+ with ND_3 gas target at energies between 17 eV and 833 eV in the center-of-mass frame. Absolute luminescence cross sections, excitation functions, and the ND(c-a)/ND(A-X) branching ratios (BR) were determined. The sum of all luminescence cross sections in the 200–600 nm spectral window is below 1×10^{-20} m^2 at 833 eV. The ND(c-a)/ND(A-X) luminescence BR increases with collision energy from BR = 0.20 at 20 eV to BR = 0.30 at 150 eV and up to 833 eV. Computer simulations of the spectra were used to estimate rotational and vibrational temperatures of the products. The population distributions of rotational and vibrational states of ND^*(A, c) do not vary appreciably with collision energy.

1 Introduction

Dissociative processes leading to the formation of excited molecules or atoms are very important in plasma chemistry, laser physics, plasma-related technologies and in the optical plasma diagnostics. The spectroscopic studies of the dissociation products and their branching into various excited states are helpful in the analysis of chemical reactions occurring in the laboratory reactors or in space, in particular in determining the abundance of ions or neutral species. Ammonia is an important molecule which is present in the atmosphere of the Sun and some its planets, mainly Jupiter, and, to a lesser degree, the Earth. Through the emission of NH^* and NH_2^* ammonia was discovered in the spectra of comets (e.g. Halley) [1,2] and in the interstellar matter [3]. Recent studies [4,5] were performed to investigate the interaction of xenon ion spacecraft thrusters with the surrounding gas containing NH_3. Ammonia can dissociate into NH_2, NH, N, H, NH_2^+, NH^+, H_2^+, N^+ ground state products [6–8], however, there are also numerous pathways leading to electronically excited fragments. A complete description of the dissociation reaction yielding excited states requires not only the identification of emitters, but also the knowledge of luminescence cross sections, preferably in the form of excitation functions. All previous studies show that the main optical signature of the ammonia dissociation is the electronic luminescence of NH molecule. The spectra of imidogen radical, NH, have been observed before in stars and other light sources in space. The electronically excited NH^* molecule can be easily formed from ammonia by a variety of physical and chemical processes.

The early studies of collision induced dissociation of ammonia used ionic atomic and molecular projectiles and involved mostly mass spectroscopic detection of the products [9–13]. The optical emission in the dissociation of NH_3 was obtained with VUV-photons from rare gas discharges (see e.g. Ref. [14,15]). More recent studies [16,17] used synchrotron radiation or other modern VUV sources. Spectroscopic control of dissociation by pumping vibrational modes with microwave photons was demonstrated in references [18–20].

There are numerous papers reporting on optical emission in collision induced dissociation (CID) of NH_3 by electrons (an excellent and comprehensive experimental work [21] contains references to all earlier studies of this system). Thermal and accelerated rare gas atoms (Ar, Kr, Xe) in the metastable $^3P_{0,2}$ states were also used as the projectiles [22–24]. Rare gas ions Ar^+, Kr^+, Xe^+, Xe^{++} colliding with NH_3 at E_{CM} up to 200 eV produced relatively intense NH^* emission [4,5]. The spectra of NH^* were also observed when NH_3 was bombarded with carbon C^+ ions or with hot neutral carbon atoms [25], for these systems the electronically excited imidogen was formed not only by collision-induced dissociation but also as a result of chemical reactions involving atom transfer. Single-electron charge transfer was studied for He^{++} collisions with NH_3 [26]. A systematic optical study of dissociation of ammonia by He^+ ions was never performed before, in the literature one can find only a brief remark [27],

[a] e-mail: s.werbowy@ug.edu.pl

that the observed NH^*(A-X, c-a) spectra in He-NH_3 afterglow are probably due to the collisions of NH_3 with helium ions. Helium He^+ ion has the highest recombination energy of all singly charged ions and the energy balance shows that, in case there are no reaction barriers involved, it should be able to produce electronically excited fragments of NH_3 molecule even at the lowest collision energies. The goal of the present study is to investigate the optical emission in the 200–600 nm spectral range for the He^+ ions colliding with ammonia at E_{CM} from 17 eV to 833 eV and in this way to extend the studies of reference [4] to the lightest rare gas ion. The recorded spectra enable measurements of luminescence cross sections and the determination of population distributions of the product states described by vibrational (T_{vib}) and rotational (T_{rot}) temperature parameters. The latter results are achieved by comparing the experimental spectra with the contours obtained by computer simulations.

A major obstacle in the determination of rotational and vibrational temperatures of NH^* products is the predissociation of the NH(A $^3\Pi$) and NH(c $^1\Pi$) states into the repulsive NH(1 $^5\Sigma^-$) state [28,29]. Thus a large part of NH^*(A, c) excited molecules is deactivated in non-radiative processes. Little affected by predissociation are only these fragments of the NH(A-X)&NH(c-a) electronic spectra which are attributed to the transitions from the $v' = 0$ vibrational state, while the emissions from $v' = 1$ are substantially weakened, and the contributions from $v' > 1$ are almost completely absent. To diminish the effect of predissociation, in the present study we use deuterated ammonia (ND_3) as the target gas. The isotopic effect on vibrational and rotational energy levels causes the ND(A-X, c-a) spectra of the products to contain more lines, as more rovibronic levels lie below the value of internal energy at which predissociation of the ND(A $^3\Pi$) and ND(c $^1\Pi$) states begins depletion of emitters.

2 Experimental

A schematic of the apparatus was the same as presented before [30]. The vacuum part was equipped with three chambers pumped differentially. The first chamber hosted a hot-cathode Colutron ion source. He^+ ions were generated from helium gas (purity 99.999%) at the ion source pressure of 20 Pa and the anode-to-cathode voltage of 50 V, to minimize the formation of electronically excited He^+ ions. Helium ions were extracted from the source by a 1000 V potential, and entered a second vacuum chamber, where they were mass-selected by a magnetic field separator. The first two chambers were pumped by 1200 L/s oil diffusion pumps equipped with liquid nitrogen traps. Subsequently, the ions were transported to the third chamber, passed through a retarder, where they were slowed down to a required energy, and entered the collision cell through a slit 1 mm wide, 10 mm high. The collision chamber was pumped by two parallel turbomolecular pumps (pumping speeds 1400 L/s and 450 L/s), which maintained the background pressure below 10^{-4} Pa during the measurements. The beam energies were in the 20–1000 eV range (transformation to the center-of-mass system, CM, requires multiplication of the laboratory beam energy by 20/24), with corresponding beam currents of 1–70 nA. The ion currents were recorded continuously with a Keithley picoammeter, digitalized, and computer-averaged. The ion beam path in the collision cell was 24 mm, of which the region between $l_1 = 6$ mm from the entrance slit and $l_2 = 18$ mm was observed by the detection system. ND_3 (Aldrich; purity 99%) gas supply was controlled through a Granville-Phillips automatic valve. The target gas pressure was measured with an MKS Baratron capacitance manometer (head type 398 HD), digitalized and computer-averaged; it was kept below 0.2 Pa, to maintain single-collision conditions. The light resulting from collisions passed through an MgF_2 window and was reflected by an aluminum mirror towards the entrance slit of a spectrograph. The luminescence spectra were recorded with a 1024-channel "Mepsicron" detector attached to a modified McPherson 218 spectrograph, which was equipped with 150, 300, 1200, and 2400 L/mm interchangeable snap-in gratings blazed at various wavelengths. The detector is sensitive only in the 200–600 nm spectral region. The sensitivity profile was determined using a standard Osram Wi17/G tungsten ribbon lamp and a Hamamatsu L656K deuterium lamp [31]. The luminescence signal was about 10–400 cts/s, depending on the ion beam energy and optical slit width used. The detector dark count rate was 2 cts/s.

To measure the luminescence intensity on the scale of absolute cross sections, we have performed several measurements for each of the two selected luminescent reactions reported in the literature: (a) for the $H^+ + N_2$ collisions at the beam energy of 1000 eV [32] and, independently, for the $He^+ + H_2$ reaction at the beam energy of 700 eV [33]. Both scaling reactions gave almost identical results.

Due to relatively large radiative lifetimes of the molecular ND^* and ND^{*+} emitters, the luminescence cross sections had to be corrected by factors accounting for escape of electronically excited products from the observation zone. Firstly, the transfer of kinetic energy from He^+ ions to the ND_3 target in the laboratory system was calculated. Secondly, we assumed that the contribution to the molecular emission comes mostly from central collisions, so the loss of light occurs only along the direction of the projectile velocity. This assumption has been checked by the observations of the collision zone with the detector in the position-sensitive mode, which enables determination of coordinates of an emitter inside the collision cell. These tests have shown that when the spectrograph slit was fully open, at beam energies above 100 eV most of the light was emitted from the observation volume determined by the entrance slit of the scattering cell. Thirdly, we have assumed that the ND^* product will have the same velocity as that acquired by ND_3 from the ion projectile. Finally, to calculate the correction factors for escape of emitters we applied the procedure described in reference [34], using the derived product velocities, dimensions of the observation zone and radiative lifetimes. The lifetime of ND(A) equals to 415 ns [35], for ND(c) it was measured to be 500 ns

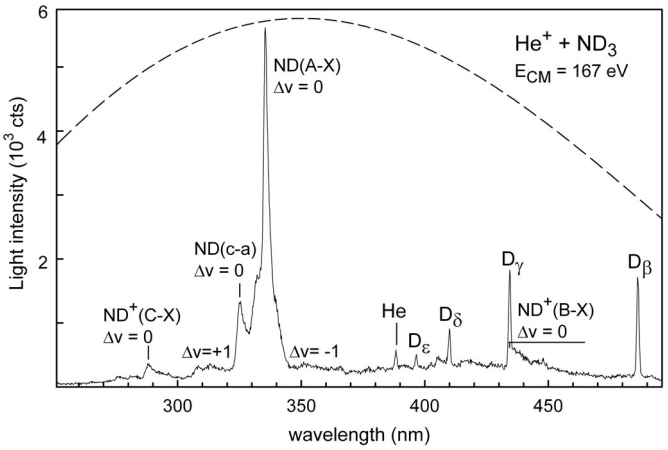

Fig. 1. Overwiew spectrum of luminescence from collisions of He^+ with ND_3 at $E_{CM} = 167$ eV recorded with spectral resolution of 0.7 nm. Spectral sensitivity of the detection system is given by dashed line.

for $v' = 0$ and about 230 ns for $v' = 1$ [36], for $ND^+(B)$ and $ND^+(C)$ we used the values given in reference [37] for the corresponding electronic states of NH^+, namely 980 ns and 400 ns, respectively.

Computer simulations of the spectra have been performed using formulas from [38] and spectroscopic data for ND (or NH) from references[1] [39–43]. Some spectroscopic constants used for ND(c-a) were derived from the data for NH(c-a) [44] using the mass-ratio rules for isotope effect [38]. For ND^+ the spectroscopic constants were taken from[1] [45–47]. The Hönl-London factors from references [48–50] were used. The Franck-Condon factors for ND(A-X) were taken from [51], for ND(c-a), ND^+(B-X), and ND^+(C-X) they were calculated using Morse potentials and spectroscopic constants from[1] [39–47]. These FCF data are available upon request.

3 Luminescence spectra

An overview spectrum obtained from collisions of He^+ with ND_3 at $E_{CM} = 167$ eV is shown in Figure 1. The dominant luminescence emitter is ND* radical, with the characteristic ND($A\ ^3\Pi - X\ ^3\Sigma^-$) and ND($c\ ^1\Pi - a\ ^1\Delta$) bands of the $\Delta v = 0$ sequence in the 320–350 nm region. Both upper states of these transitions converge to the same $N(^2D) + D(^2S)$ asymptote and predissociate to the repulsive $ND(1\ ^5\Sigma^-)$ state. In the ND(A-X) spectrum only four vibrational states ($v' = 0$–3) are observed, the ND(c-a) transition has a clear ($v' = 0 \rightarrow v'' = 0$) band, while the (1, 1) band is weakened by predissociation (the ND(c; $v' = 1$) state has the radiative lifetime $\tau = 236$ ns, which is less than half of τ for $v' = 0$). The ND^+(B-X) ($\Delta v = 0$) transition can be recognized on the right side of the Balmer D_γ atomic line, however, the entire ND^+(B-X) spectrum, with other, less intense bands of other sequences, covers the wavelength region from 380 nm to 510 nm and probably contributes to the rise of the background in this area. Below 320 nm one can identify the ND^+(C-X) transition. The Balmer series for deuterium atom is also present, as well as the strongest He line at 388.8 nm, which arises from the $He(3\ ^3P)$ state[1]. One has to keep in mind that the molecular species observed in this experiment have different lifetimes of excited states, therefore various products have different rates of escape from the observation zone and this in turn changes the apparent relative light intensities of molecular bands. We found that the best conditions for simultaneous demonstration of all molecular emitters exist at the collision energy just below 200 eV.

The observed luminescent product channels are listed below in the order of calculated energy balance ΔE_0, which was obtained for the lowest vibrational and rotational levels of molecular species. A negative value of the energy balance ΔE_0 means that the channel is exoergic,

$$
\begin{aligned}
&He^+(^2P) + ND_3(X\ ^1A_1) \rightarrow \\
&\rightarrow He(^1S) + ND^{+*}(B\ ^2\Delta) + D_2(X\ ^1\Sigma_g^+), \\
&\Delta E_0 = -4.1 \text{ eV}, && (1) \\
&\rightarrow He(^1S) + ND^{+*}(C\ ^2\Sigma^+) + D_2(X\ ^1\Sigma_g^+), \\
&\Delta E_0 = -2.7 \text{ eV}, && (2) \\
&\rightarrow He(^1S) + ND^*(A\ ^3\Pi) + D_2^+(^2\Sigma_g^+), \\
&\Delta E_0 = -1.1 \text{ eV}, && (3) \\
&\rightarrow He(^1S) + ND^{+*}(B\ ^2\Delta) + D(^2S) + D(^2S), \\
&\Delta E_0 = 0.4 \text{ eV}, && (4) \\
&\rightarrow He(^1S) + ND^*(c\ ^1\Pi) + D_2^+(^2\Sigma_g^+), \\
&\Delta E_0 = 0.5 \text{ eV}, && (5) \\
&\rightarrow He(^1S) + ND^*(A\ ^3\Pi) + D(^2S) + D^+, \\
&\Delta E_0 = 1.6 \text{ eV}, && (6) \\
&\rightarrow He(^1S) + ND^{+*}(C\ ^2\Sigma^+) + D(^2S) + D(^2S), \\
&\Delta E_0 = 1.9 \text{ eV}, && (7) \\
&\rightarrow He(^1S) + ND^*(c\ ^1\Pi) + D(^2S) + D^+, \\
&\Delta E_0 = 3.2 \text{ eV}, && (8) \\
&\rightarrow He(^1S) + ND_2^+(X\ ^3\Sigma^-) + D^*(4l), \\
&\Delta E_0 = 4.4 \text{ eV}, && (9) \\
&\rightarrow He^*(3\ ^3P) + ND_3^+(X\ ^2A_2''), \\
&\Delta E_0 = 8.5 \text{ eV}, && (10) \\
&\rightarrow He(^1S) + ND(X\ ^3\Sigma^-) + D^*(4l) + D^+, \\
&\Delta E_0 = 10.5 \text{ eV}, && (11) \\
&\rightarrow He^{+*}(4d\ ^2D) + ND_3(X\ ^1A_1), \\
&\Delta E_0 = 50.0 \text{ eV}. && (12)
\end{aligned}
$$

The above channels mostly describe collisional dissociation of the target, one exception is channel (10), which denotes a charge transfer with excitation of the neutralized projectile ion, the other exception is channel (12),

[1] http://webbook.nist.gov/cgi/cbook.cgi?ID=C15123009\&Units=SI\&Mask=1000

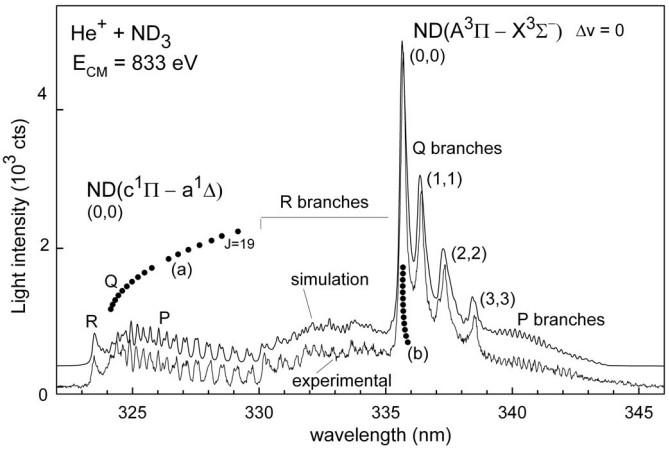

Fig. 2. Luminescence spectra of ND(A-X, c-a) in the region of $\Delta v = 0$ sequence, obtained in the collisions of He^+ with ND_3 at $E_{CM} = 833$ eV and recorded with spectral resolution of 0.13 nm. The simulated spectrum is shifted upwards for a better comparison. The full circles mark two groups of selected rotational lines identified in [41] and in [42]; the groups are described as (a) and (b), respectively.

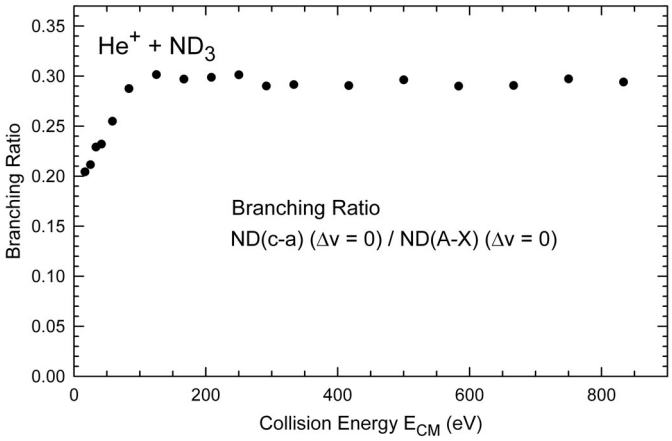

Fig. 3. The branching ratio of intensities ND(c-a)/ND(A-X) observed in the spectra for the $\Delta v = 0$ sequences of the electronic transitions.

corresponding to collision-induced excitation of the projectile ion. We do not see any evidence of emission from the following product channels:

$$\rightarrow \mathrm{He}(^1\mathrm{S}) + \mathrm{ND}^{+*}(\mathrm{A}^2\Sigma^-) + \mathrm{D}_2(\mathrm{X}^1\Sigma_g^+)$$
$$\Delta E_0 = -4.5 \text{ eV}, \quad (13)$$
$$\rightarrow \mathrm{He}(^1\mathrm{S}) + \mathrm{ND}_2^*(\widetilde{\mathrm{A}}^2\mathrm{A}_1) + \mathrm{D}^+$$
$$\Delta E_0 = -4.6 \text{ eV}. \quad (14)$$

Extremely weak luminescence by these two emitters, $ND^{+*}(A)$ and $ND_2^*(A)$, was observed during ammonia bombardment by electrons [21]. NH_3^+ does not show emission spectrum in the UV-Vis region [52].

All the processes (1)–(14) satisfy the spin conservation rule. The most exothermic channels of all listed above are (13) and (14), however, in the recorded spectra their known spectral features are absent. The ND^+(A-X) emission should lie on top of the ND^+(B-X) spectrum, but the appearance of its $\Delta v = 0$ sequence is possibly weakened due to a large difference in equilibrium distances of the electronic states involved, Δr_e. In addition, $ND^{+*}(A)$ has a longer lifetime ($\tau = 1080$ ns) [37] than $ND^{+*}(B)$ ($\tau = 980$ ns) and therefore a higher probability to escape from the observation zone. In the past, the ND^+(A-X) transition was not observed in similar spectroscopic studies using accelerated ion beams, while the ND^+(B-X) transition was relatively strong [45,53]. The $ND_2(\widetilde{A}\ ^2A_1 - X\ ^2B_1)$ transition usually gives a broad "quasi-continuum" spectrum in the 300–500 nm region. The main obstacle in recording the spectrum is a long radiative lifetime of $ND_2^*(\widetilde{A}\ ^2A_1)$, as for $NH_2^*(\widetilde{A}\ ^2A_1)$ it is about 10 μs [54]. In our arrangement, a lifetime of this order allows for a massive (>98%) escape of emitters from the observation window.

A fragment of the ND^* spectrum containing the $\Delta v = 0$ sequences of ND(A-X) and ND(c-a) transitions is shown in Figure 2. For a better understanding of the band structure, the wavelengths of selected groups of rotational lines are marked as (a) and (b). These lines were earlier identified in the Q-branches of ND(c-a)(0, 0) and ND(A-X)(0, 0) in references [41,42], respectively. The ND(c-a)($\Delta v = 0$) spectrum is partially superimposed by the ND(A-X) ($\Delta v = 0$) emission, therefore after corrections for detector sensitivity, the sum of photons at wavelengths below 330 nm was found (which can be attributed only to the ND(c-a) ($\Delta v = 0$) system), to which some photons emitted above 330 nm were added. This latter contribution was estimated using computer simulated spectral contours generated for both electronic transitions. The intensities of light were corrected for escape of emitters. The derived branching ratios are given in Figure 3. One can see that after a slow increase from BR = 0.20 to BR = 0.30, the branching ratio stabilizes at the latter value up to 833 eV. This behavior of BR can be explained by the fact that the ND(A) and ND(c) electronic states of ND derive from the related singlet-triplet pair of ND_3^* excited states of essentially the same energy [55]. The value of the branching ratio reflects the statistical weight of singlet (c $^1\Pi$) to triplet (A $^3\Pi$) populations, which should be 1:3. This hypothetical 0.33 ratio is slightly disturbed at low E_{CM} by a factor resulting from available volume of phase space, with favors more exoergic states. When the contributed collision energy is lower, some deficit of ND(c) production vs. the ND(A) state population occurs, because the former state lies 1.65 eV above the latter. The BR values were often reported for other systems. For Ar^+, Kr^+, and $Xe^+ + NH_3$, the branching ratio is 0.10 (at 69 eV), 0.07 (at 101 eV), and 0.04 (at 69 eV), respectively [4]. The authors proposed that the observed decrease of BR values with increasing ion mass for Ar^+, Kr^+, and Xe^+ occurs because the NH^*(c) and NH^*(A) molecules are formed via two different mechanisms, although both involving excitation of ammonia, which subsequently dissociates [4]. One has to keep

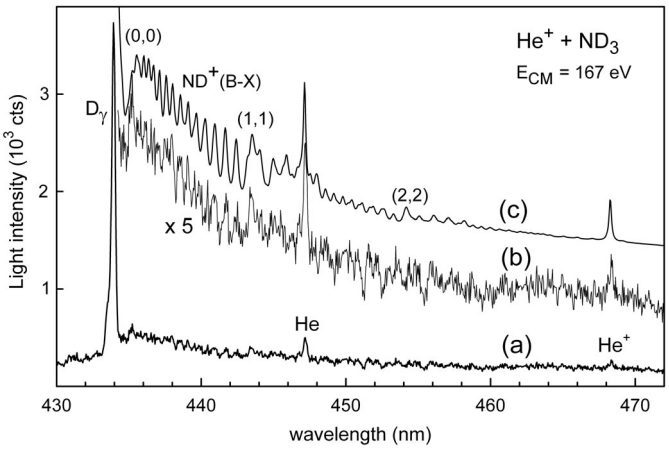

Fig. 4. Luminescence of ND^+(B-X) in the region of $\Delta v = 0$ sequence. Collision energy $E_{CM} = 167$ eV, spectral resolution 0.35 nm. Trace (a) shows the atomic D_γ line of the hydrogen Balmer series together with the molecular spectrum, trace (b) gives the molecular spectrum with intensity expanded by the factor of 5, trace (c) is the computer simulated spectrum, shifted upwards for a better comparison. The He and He^+ lines are at 447.1 nm and 468.5 nm, respectively.

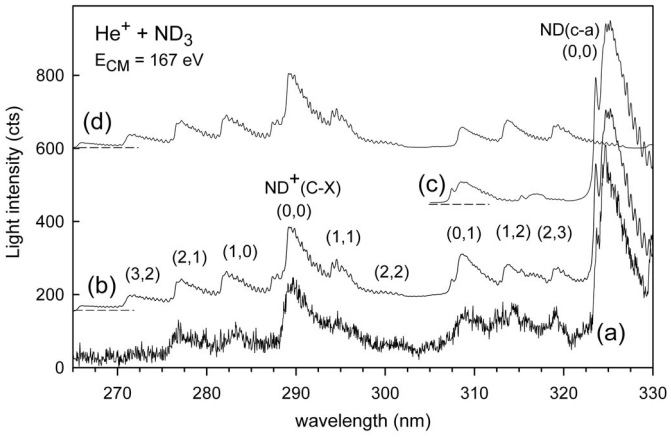

Fig. 5. Trace (a): luminescence in the 265–330 nm region at $E_{CM} = 167$ eV, spectral resolution 0.35 nm; trace (b): simulated spectrum including all emitters; trace (c): simulated contribution of ND(c-a); trace (d): simulated contribution of ND^+(C-X).

in mind that in some experiments cited above (photodissociation, electron bombardment) the spin-conservation rule blocks channels leading to NH(A $^3\Pi$) + H_2 and this strongly modifies the NH(c/A) product branching ratio. For e^- + NH_3 collisions the measured BR(NH(c/A)) = 0.95 at 22 eV and BR = 1.9 at 92 eV [56]; a more reliable result seems to be BR = 0.75 at 100 eV [21]. For thermal $Ar^*(^3P)$ + NH_3 collisions it was found BR = 0.31 in the afterglow and BR = 0.28 in a low-pressure free jet [23], while for $Ar^*(^3P)$ + NH_3 at slightly elevated collision energies (up to 1.5 eV) the observed BR was between 0.6 and 1.0; it increased to the value between 1.0 and 1.6 after corrections for predissociation [24]. From the comparison of BR for various systems, one can see that these results are strongly dependent on the choice of the projectile.

Figure 4 contains the $\Delta v = 0$ sequence of the ND^+(B-X) transition observed experimentally (trace (a)), the same spectrum expanded by the factor of five (trace (b)), and a computer simulation of the latter (trace (c)). Figure 5 presents the recorded spectrum in the 265–330 nm wavelength region (trace (a)), the simulated spectrum (trace (b)), and the partial contributions to the simulated spectrum: a superimposed fragment of ND(c-a) emission (trace (c)) and the contribution of ND^+(C-X) (trace (d)).

The experimental spectra could be successfully simulated using rotational and vibrational temperatures given in Table 1 [4,14,21,23,24,57,58]. For collision energies in the 70–833 eV range, the shape of the ND* spectrum is essentially the same. Temperatures describing populations of the ND(A) and ND^*(c) products are independent of collision energy, although for the A-state they are higher than for the c-state. For the He^++ ND_3, the computer simulation requires also an individual adjustment of T_{rot} for each vibrational level of ND^*(A). The rotational and vibrational temperatures in Table 1 correspond, with one exception, to only a fraction of eV (*ca.* 0.1–0.5 eV). Estimates of the temperatures of analogous products obtained when NH_3 has been dissociated by other projectiles (see the footnotes in Tab. 1) are mostly similar to these obtained in the present work. The vibrational temperature for ND^+(C) is an exception from typical values of T_{vib} for neutral products, and suggests a different excitation mechanism.

4 Luminescence cross sections

The apparent excitation function for the emission observed from the $\Delta v = 0$ sequences of ND(A-X) and ND(c-a) in the 323–346 nm spectral region is shown in Figure 6 by a dashed line and open circles. For collision energies above 50 eV this function required a correction for escape of emitters from the observation zone (the procedure is described in the experimental section). After the correction, the excitation function (drawn as a continuous line, full circles) preserves a local maximum at *ca.* 70 eV, while above 100 eV it increases monotonically. A somewhat different shape of the excitation function for NH* has been observed for e^- + NH_3 [21,57,59]; in reference [21] a maximum at 24 eV (for A-X) and at 70 eV (for c-a) is followed by a slow decrease up to 1000 eV, to a σ^*-value near 30% of the maximum.

We attribute the production of ND^*(A, c) emitters to the collision-induced dissociation of the target by He^+ ions. The dissociation can occur after the electron transfer from the target to He^+ projectile ion but also when the charge transfer fails. The latter scenario requires somewhat higher input of collision energy (for production of ND^*(A) the deficit is ΔE_0 = 8.03 eV). From photodissociation experiments and ab initio study for NH_3 and ND_3 [60] it is known that the first excited singlet state of ND_3(A) predissociates into ND_2 + D with very high efficiency and about 3% of the ND_2 products

Table 1. Rotational and vibrational temperatures of the products determined from the observed spectra for the He^++ND_3 system.

Collision energy /Spectral resolution	Product/transition	Rotational temperature T_{rot}	Vibrational temperature T_{vib}
1000 eV (0.13 nm)	ND(A-X) ($\Delta v = 0$)	for $v' = 0$, 1, 2, 3: T_{rot} = 4000 K, 3000 K 2500 K, 1000 K[(a,b,c,d,e)]	4600 K[(f)]
1000 eV (0.13 nm)	ND(c-a) ($\Delta v = 0$)	1400 K[(g,h,i,j,k,l)]	2000 K
200 eV (0.7 nm)	ND(A-X) (all (v', v"))	3200 K[(m)]	4600 K[(n)]
200 eV (0.7 nm)	ND(c-a) (all (v', v"))	1400 K	3000 K
200 eV (0.35 nm)	ND^+(B-X) ($\Delta v = 0$)	1500 K[(o)]	4000 K
200 eV (0.35 nm)	ND^+(C-X) (all (v', v"))	3000 K[(p)]	>20 000 K

[(a)] $e^- + NH_3$ ($E_{coll} = 70$ eV): $T_{rot} = 1730$ K [58]; [(b)] $e^- + NH_3$ (120 eV): non-boltzmann population, approx. $T_{rot} = 8000$ K [56]; [(c)] $e^- + NH_3$ (100 eV): non-boltzmann population, mixture $T_{rot} = 4500$ K (60%) and 9000 K (40%) [21]; [(d)] thermal $Ar^*(^3P_{0,2}) + NH_3$: $T_{rot}(v' = 0) = (2000\pm500)$ K, T_{rot}(v' = 1) = (1000 ± 200) K [23]; [(e)] $Ar^*(^3P_{0,2}) + NH_3$ (1.4 eV): $T_{rot} = (2000\pm750)$ K [24]; [(f)] $e^- + NH_3$ (70 eV): $T_{vib} = 4000$ K [58]; [(g)] photodissociation of NH_3: $T_{rot} = 6000$ K [14]; [(h)] $e^- + NH_3$ (120 eV): $T_{rot} = (1690 \pm 100)$ K [56]; [(i)] $e^- + NH_3$ (100 eV): $T_{rot} = 1240$ K [57]; [(j)] $e^- + NH_3$ (100 eV): $T_{rot} = 2000$ K [24]; [(k)] thermal $Ar^*(^3P_{0,2}) + NH_3$: $T_{rot}(v' = 0) = (900 \pm 200)$ K [23]; [(j)] $Ar^*(^3P_{0,2}) + NH_3$ (1.4 eV): $T_{rot} = 900$ K [24]; [(l)] $e^- + NH_3$ (100 eV): $T_{rot} = 2000$ K [21]; [(m)] $Xe^+ + NH_3$ (103 eV): $T_{rot} = 4200$ K [4]; [(n)] $Xe^+ + NH_3$ (103 eV): $T_{vib} = 3050$ K [4]; [(o)] $e^- + NH_3$ (100 eV): $T_{rot} = 3000$ K [21]; [(p)] $e^- + NH_3$ (100 eV): $T_{rot}(v' = 0) = 3000$ K, $T_{rot}(v' = 1) = 5000$ K [21].

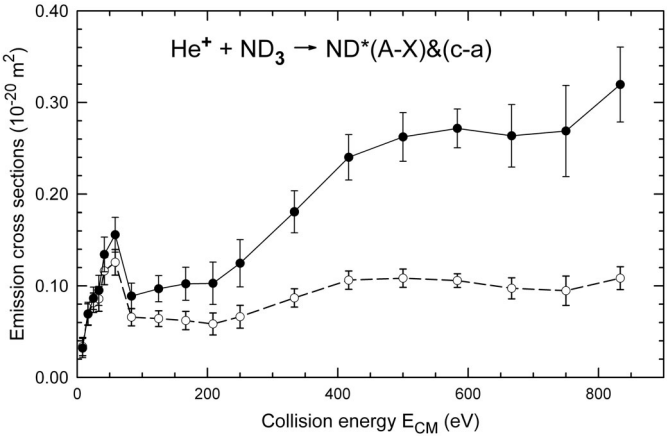

Fig. 6. Excitation function for ND(A-X) and (c-a) obtained directly from experiment (open circles, dashed line) and corrected for escape of emitters from the observation zone (full circles, continuous line).

are in the excited state. At higher energies the dissociation has more available channels leading to ND*. Theoretical work [55] gave calculated SCF potential curves for the abstraction process $NH_3 \rightarrow NH^* + H_2$, which were later used in the interpretation of results obtained for e^- + NH_3 [21], RG* + NH_3 [23], and RG^{+*} + NH_3 [4]. The NH_3 molecule in the ground state X $^1A_1$ pyramidal conformation of C_{3v} symmetry has the $(1a_1)^2(2a_1)^2(1e)^4(3a_1)^2$ electronic configuration. In the first excited state NH_3(A), arising from the $3a^1 \rightarrow 3s$ Rydberg-type electron promotion, ammonia is planar and has D_{3h} symmetry. In this new conformation, two electronic states, namely A $^3A_2''$ and A $^1A_2''$, are about 0.3 eV apart and about 6.3 eV above the ground state of NH_3(X $^1A_1'$). In the dissociation process, two hydrogen atoms form H_2 in C_{2v} symmetry; this step creates energy barriers, which are somewhat different for the singlet and triplet surfaces. After surmounting the barriers, the system evolves towards product states correlating with the NH^*(A $^3\Pi$) + H_2 (releasing about 2.2 eV) and NH^*(c $^1\Pi$) + H_2 (releasing about 0.8 eV) asymptotes. The measured temperatures reflect these values, if we assume a statistical distribution of energy among all degrees of freedom of the products. Higher excited states of NH_3^* lead to the NH^*(A, c) + 2H(^{2}S) products. This mechanism of ND^*(A) and ND^*(c) formation corresponds well with the observed independence of ND^* spectra on collision energy. The maximum at lower energies in Figure 6 can be due to the formation of unstable excited states of the target, which was suggested for He^+ + NH_3 below $E_{CM} = 100$ eV [12]. In the same spirit, other studies [17] point out that after the VUV excitation of ammonia above 15.6 eV, there is a possibility of conversion from long-lived NH_3^* into NH_2^* with even longer lifetime. The altering of the intermediate species could have therefore contributed to the appearance of the maximum in Figure 6.

For e^- + NH_3 at collision energy of 100 eV, reference [21] gives σ^*(A-X, c-a) = $(0.049 \pm 0.005) \times 10^{-20}$ m^2, the same as the result in reference [61]. For Xe^+ + NH_3 at $E_{CM} = 100$ eV, the NH(A-X) emission cross section is about 0.1×10^{-20} m^2 [4]. Our result at this collision energy is almost identical, although at lower E_{CM} we found a maximum, while the Xe^+ projectile gives only a little shoulder on the excitation function. The total charge transfer cross section for He^+ + NH_3 is $\sigma_{CT} = 10 \times 10^{-20}$ m^2, and it is almost constant throughout the range of collision energies between 80 eV and 1000 eV [12]. Assuming the same σ_{CT} for the deuterated

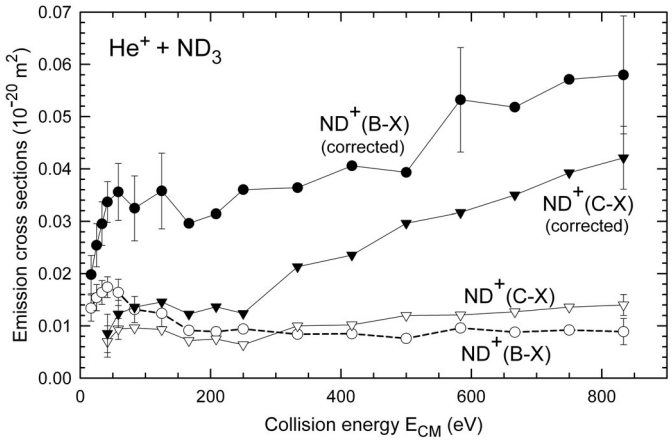

Fig. 7. Excitation functions for ND^+(B-X) ($\Delta v = 0$) (circles) and ND^+(C-X) ($\Delta v = 0$) (triangles) obtained directly from the spectra (open symbols) and corrected for escape from the observation zone (full symbols).

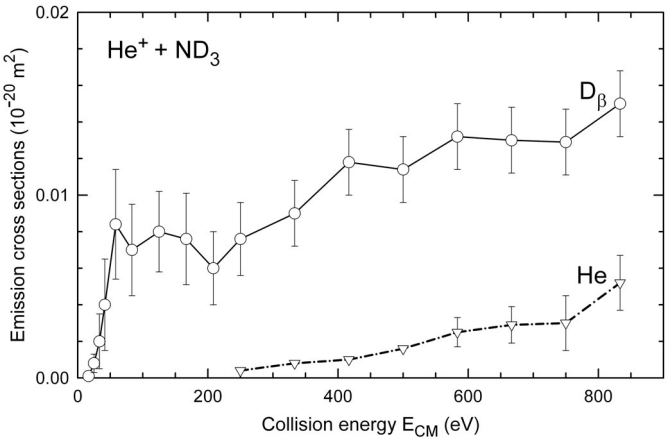

Fig. 8. Excitation functions for the D_β line of the Balmer series and for He 388.8 nm atomic line.

ammonia target, the luminescence cross section σ^*(A-X, c-a) obtained in the present work at $E_{CM} = 833$ eV corresponds to the luminescence yield $\Phi = \sigma^*/\sigma_{CT} = 3\%$.

For the ND^+(B-X) ($\Delta v = 0$) and ND^+(C-X) ($\Delta v = 0$) emissions the excitation functions are shown in Figure 7. The open symbols denote the cross sections derived from the measured light intensities, which suggest that for higher collision energies there is more light from the C-X transition than from the B-X transition, this is however an artifact. The full symbols mark the cross sections after corrections for escape of emitters (see experimental section). Since the radiative lifetime of ND^+(B) is much longer than that of ND^+(C), the σ^*(B)-excitation function is above that of σ^*(C) at all collision energies. The low-energy ends of the excitation functions resemble those presented in [21] for $e^- + NH_3$, where for both excited states, $NH^+(B\ ^2\Delta)$ and $NH^+(C\ ^2\Sigma^-)$, a maximum of σ^* is reached at about 70 eV. Excitation functions with a distinct maximum at 70 eV have been observed also in the experimental studies of NH_2^+ and NH^+ production in the dissociative ionization of ammonia by electron impact [62,63]. For higher collision energies, the NH^{+*}(B, C) cross sections decrease in [21], while in the present work for ND^{+*}(B, C) they increase (see Fig. 7). Although the ND^{+*}(B, C) products are formed in the most exoergic channels observed, (1) and (2), the corresponding luminescence cross sections are substantially smaller than these for the ND^*(A, c) products. Relative cross sections for the NH_3^+, NH_2^+, and NH^+ products of Ar^+, $Kr^+ + NH_3$ collisions at 500 eV were measured in reference [8]. The NH^+ fraction (both, unexcited and excited molecules) was found to be about 2% and the author concluded that the product channel was the energetically higher $NH^+ + 2H$, rather than $NH^+ + H_2$. Absolute emission cross sections measured for $e^- + NH_3$ at 100 eV are about 0.002×10^{-20} m^2 and 0.0007×10^{-20} m^2 for NH^{+*}(B) and NH^{+*}(C), respectively [21], i.e. they are an order of magnitude lower than the corresponding ones obtained in the present work.

The excitation function for Balmer D_β ($n = 4 \rightarrow n = 2$) line is given in Figure 8. At collision energy of 100 eV the absolute cross section for D_β produced in $He^+ + ND_3$ is nearly the same as that for the $e^- + NH_3$ system [57,61]. The shape of excitation function, however, is similar only in reference [57], showing an increase of H_β intensity with collision energy, while reference [61] reports that the intensity of this atomic line decreases with collision energy. The components of the Balmer-β line have upper states $4l$ with lifetimes no longer than 227 ns [64] and there is no need to apply a correction for escape of emitters. A direct proof of the charge exchange between He^+ and ND_3 is the He 388.8 nm line. The excitation function of this line is presented in Figure 8. Equation (10) gives the energy balance for a hypothetical He^+ neutralization process that requires minimum energy to possibly observe this He line, however, the excitation function indicates that much higher collision energies are required to populate this He state, likely via a channel involving dissociation of the target molecule.

5 Conclusions

Numerous electronic transitions in diatomic molecules and atoms, both neutral and ionic, have been observed as the result of dissociation of deuterated ammonia ND_3 by impact of accelerated He^+ ions. The dominant light emitter is the ND^*(A, c) molecule. The excited imidogen can be produced in collision-induced dissociation of the target by He atoms formed via charge exchange, but also by a fraction of He^+ ions which were not neutralized. The similarity of the spectra and almost identical vibrational and rotational temperatures of ND^*(A, c) products at all collision energies studied, support the view that the emitters are formed by electron promotion in the ND_3 molecule. The results indicate statistical electronic branching ratio for the ND^*(c/A) states. The available kinetic energy seems to play little role in the collision dynamics after the thresholds for luminescent processes have been overcome.

Other observed emitters are the ND^{+*}(B, C) cation, the D* atom, and He^*, He^{+*} atoms. All luminescence cross sections increase with collision energy up to 833 eV, but the sum of all σ^* remains below 1×10^{-20} m^2 at the highest energy. The excitation functions determined for the first time in the present work can be useful in modelling processes in plasma containing helium and ammonia, they are also important for the analysis of reaction kinetics in cosmochemistry.

This work was financed within the statutory fund DS-530-5200-D464-16 and from the research project of the Polish National Science Centre (Polskie Narodowe Centrum Nauki, abbrev. NCN), DEC-2012/05/D/ST9/03912.

Author contribution statement

All authors contributed equally to the paper.

References

1. S. Wyckoff, S. Tegler, L. Engel, Adv. Space Res. **9**, 169 (1989)
2. V. Guineva, R. Werner, Adv. Space Res. **40**, 155 (2007)
3. P.T.P. Ho, C.H. Townes, Ann. Rev. Astron. Astrophys. **21**, 239 (1983)
4. B.D. Prince, C.P. Steiner, Y.-H. Chiu, J. Chem. Phys. **136**, 144314 (2012)
5. D.J. Levandier, Y.-H. Chiu, J. Chem. Phys. **133**, 154304 (2010)
6. M.A. Coplan, K.W. Oglivie, J. Chem. Phys. **52**, 4154 (1970)
7. S.P. Khare, S. Prakash, W.J. Meath, Int. J. Mass Spectrom. Ion Proc. **88**, 299 (1989)
8. E. Lindholm, Z. Naturforsch. **9a**, 535 (1954)
9. N.G. Adams, D. Smith, E. Alge, J. Phys. B: Atom. Molec. Phys. **13**, 3235 (1980)
10. G.R. Hertel, W.S. Koski, J. Am. Chem. Soc. **86**, 1683 (1964)
11. D.W. Koopman, Phys. Rev. **178**, 161 (1969)
12. D.W. Koopman, J. Chem. Phys. **49**, 5203 (1968)
13. W. Lindinger, D.L. Albritton, F.C. Fehsenfeld, J. Chem. Phys. **62**, 4957 (1975)
14. K.H. Becker, K.H. Welge, Z. Naturforsch. **19a**, 1006 (1964)
15. H. Okabe, *Photochemistry of small molecules* (Wiley-Interscience Publications, New York, 1978)
16. D. Edvardsson, P. Baltzer, L. Karlsson, B. Wannberg, D.M.P. Holland, D.A. Shaw, E.E. Rennie, J. Phys. B **32**, 2583 (1999)
17. Y. Song, X.M. Quian, K.C. Lau, C.Y. Ng, J. Liu, W. Chen, J. Chem. Phys. **115**, 2582 (2001)
18. A. Bach, J.M. Hutchinson, R.J. Holiday, F.F. Crim, J. Chem. Phys. **118**, 4955 (2002)
19. H. Akagi, K. Yokoyama, A. Yokoyama, J. Chem. Phys. **118**, 3600 (2003)
20. H. Akagi, K. Yokoyama, A. Yokoyama, J. Chem. Phys. **120**, 4696 (2004)
21. D. Müller, G. Schulz, J. Chem. Phys. **96**, 5924 (1992)
22. D.H. Stedman, J. Chem. Phys. **52**, 3966 (1970)
23. H. Sekiya, N. Nishiyama, M. Tsuji, Y. Nishimura, J. Chem. Phys. **86**, 163 (1987)
24. K. Tabayashi, K. Shobatake, J. Chem. Phys. **84**, 4930 (1986)
25. Ch. Ottinger, A. Kowalski, J. Phys. Chem. **106**, 8296 (2002)
26. M. Farnik, Z. Herman, T. Ruhaltinger, J.P. Toennies, J. Chem. Phys. **103**, 3495 (1995)
27. C.B. Collins, W.W. Robertson, J. Chem. Phys. **40**, 701 (1964)
28. D. Patel-Misra, G. Parlant, D.G. Sauder, D.R. Yarkony, P.J. Dagdigian, J. Chem. Phys. **94**, 1913 (1991)
29. G. Parlant, P.J. Dagdigian, D.R. Yarkony, J. Chem. Phys. **94**, 2364 (1991)
30. A. Ehbrecht, A. Kowalski, Ch. Ottinger, Int. J. Mass Spectrom. Ion Processes **156**, 41 (1996)
31. Th. Glenewinkel-Meyer, B. Müller, Ch. Ottinger, H. Tischer, J. Chem. Phys. **88**, 3475 (1988)
32. B. Van Zyl, M.W. Gealy, H. Neumann, Phys. Rev. A **28**, 2141 (1983)
33. R.C. Isler, R.D. Nathan, Phys. Rev. A **6**, 1036 (1972)
34. Ch. Ottinger, *Electronically chemiluminescent ion – molecule reactions*, in: *Gas Phase Ion Chemistry*, edited by M.T. Bowers (Academic Press, Orlando, 1984), Vol. 3
35. R.D. Kenner, A. Kaes, R.K. Browarzik, F. Stuhl, J. Chem. Phys. **91**, 1440 (1989)
36. B. Bohn, F. Stuhl, G. Parlant, P.J. Dagdigian, D.R. Yarkony, J. Chem. Phys. **96**, 5059 (1992)
37. J. Brzozowski, N. Elander, P. Erman, M. Lyyra, Phys. Scr. **10**, 241 (1974)
38. G. Herzberg, *Molecular Spectra and Molecular Structure, vol. I: Spectra of Diatomic Molecules* (Van Nostrand – Reinhold, New York, 1965)
39. K.P. Huber, G. Herzberg, *Molecular Spectra and Molecular Structure. IV. Constants of Diatomic Molecules* (Van Nostrand, New York, 1979)
40. R.S. Ram, P.F. Bernath, JOSA B **3**, 1170 (1986)
41. G.H. Dieke, R.W. Blue, Phys. Rev. **45**, 395 (1934)
42. P. Bollmark, I. Kopp, B. Rydh, J. Mol. Spectrosc. **34**, 487 (1970)
43. R.S. Ram, P.F. Bernath, J. Mol. Spectrosc. **176**, 329 (1996)
44. W. Ubachs, G. Meyer, J.J. ter Meulen, A. Dymanus, J. Mol. Spectrosc. **115**, 88 (1986)
45. I. Kusunoki, Ch. Ottinger, J. Chem. Phys. **80**, 1872 (1984)
46. R. Colin, A.E. Douglas, Can. J. Phys. **46**, 61 (1968)
47. R. Colin, J. Mol. Spectrosc. **136**, 387 (1987)
48. I. Kovács, *Rotational Structure in the Spectra of Diatomic Molecules* (Adam Hilger Ltd, London, 1969)
49. A. Budó, Z. Phys. **105**, 579 (1937)
50. L.T. Earls, Phys. Rev. **48**, 423 (1935)
51. P.W. Fairchild, G.P. Smith, D.R. Crosley, J.B. Jeffries, Chem. Phys. Lett. **107**, 181 (1984)
52. G. Dujardin, S. Leach, Can. J. Chem. **63**, 1386 (1985)
53. A. Ehbrecht, A. Kowalski, Ch. Ottinger, Int. J. Mass Spectrom. Ion Processes **173**, 127 (1998)
54. J.B. Halpern, G. Hancock, L. Lenzi, K.H. Welge, J. Chem. Phys. **63**, 4808 (1975)

55. R. Runau, S.D. Peyerimhoff, R.J. Buenker, J. Mol. Spectrosc. **68**, 253 (1977)
56. I. Tokue, M. Iwai, Chem. Phys. **52**, 47 (1980)
57. T. Sato, F. Shibata, T. Goto, Chem. Phys. **108**, 147 (1986)
58. H. Bubert, F.W. Froben, J. Phys. Chem. **75**, 769 (1971)
59. K. Fukui, I. Fujita, K. Kuwata, J. Phys. Chem. **81**, 1252 (1977)
60. M.I. McCarthy, P. Rosmus, H.-J. Werner, P. Botschwina, V. Vaida, J. Chem. Phys. **86**, 6693 (1987)
61. J.M. Kurepa, M.D. Tasič, Z.L. Petrović, Chem. Phys. **130**, 409 (1989)
62. A. Crowe, J.W. McConkey, Int. J. Mass Spectrom. Ion Phys. **24**, 181 (1977)
63. K. Bederski, L. Wojcik, B. Adamczyk, Int. J. Mass Spectrom. Ion Phys. **35**, 171 (1980)
64. A.A. Radzig, B.M. Smirnov, *Reference Data on Atoms, Molecules and Ions* (Springer, Berlin, 1985)